

## Article

# Multi-Phase Equilibrium Model of Oxygen-Enriched Lead Oxidation Smelting Process Based on Chemical Equilibrium Constant Method

Xinzhou Chen, Mingzhou Li \*, Fupeng Liu \*, Jindi Huang  and Minghao Yang

Faculty of Materials Metallurgy and Chemistry, Jiangxi University of Science and Technology, Kejia Road No. 156, Ganzhou 341000, China

\* Correspondence: [jsxstlmz@163.com](mailto:jsxstlmz@163.com) (M.L.); [fupengliu@126.com](mailto:fupengliu@126.com) (F.L.)

**Abstract:** With the increasingly complicated sources of lead smelting materials, it is becoming more difficult to optimize process parameters during the bottom-blowing lead oxidation smelting process. Building a bottom-blowing lead smelting thermodynamic model has significant importance for the green production of the lead smelting process. In this study, we built a multi-phase equilibrium thermodynamic model and simulation system for the oxygen-enriched bottom-blowing lead oxidation smelting process using the MetCal software platform (MetCal v7.81) according to the chemical equilibrium constant method. The equilibrium products composition and important technical indicators were calculated under factory operating conditions. Compared with the industrial data, the calculation results demonstrated that the average relative error of the calculation value of the mass fraction in the crude lead, lead-rich slag, and dust was 3.76%. The average relative error of important technical indicators, including dust rate, crude lead yield, lead-rich slag temperature, slag iron–silica ratio ( $R_{\text{Fe}/\text{SiO}_2}$ ), and slag calcium–silica ratio ( $R_{\text{CaO}/\text{SiO}_2}$ ), was 6.39%. As a result, the developed modeling and simulation system was able to reflect the current state of the oxygen-enriched bottom-blowing lead smelting. It also demonstrated the potential to enhance the smelting process and optimize the process parameters. Therefore, it is expected to provide a useful tool for thermodynamic analysis.



**Citation:** Chen, X.; Li, M.; Liu, F.; Huang, J.; Yang, M. Multi-Phase Equilibrium Model of Oxygen-Enriched Lead Oxidation Smelting Process Based on Chemical Equilibrium Constant Method. *Processes* **2023**, *11*, 3043. <https://doi.org/10.3390/pr11103043>

Academic Editors: Andrew S. Paluch and Haiping Zhu

Received: 7 September 2023

Revised: 15 October 2023

Accepted: 20 October 2023

Published: 23 October 2023



**Copyright:** © 2023 by the authors. Licensee MDPI, Basel, Switzerland. This article is an open access article distributed under the terms and conditions of the Creative Commons Attribution (CC BY) license (<https://creativecommons.org/licenses/by/4.0/>).

**Keywords:** lead pyrometallurgy; oxygen-enriched bottom-blowing smelting process; multi-phase equilibrium; MetCal; simulation

## 1. Introduction

The main production process for primary lead is pyrometallurgy [1]. The mainstream processes of lead smelting include bottom-blowing (SKS) [2], Queneau–Schuhmann–Lurgi (QSL) [3], oxygen-enriched side-blowing [4], Ausmelt [5], Isasmelt [6,7], Kivcet [8], and Outokumpu. Among them, the bottom-blowing smelting process, also known as the SKS technique, was developed by China Enfi Engineering Technology Co., Ltd. in 1998. Because of its advantages of wide adaptability of raw materials, low energy consumption, and environmental friendliness, this process occupies an important position in China’s lead smelting process. As a result of the complicated sources of raw materials and variable compositions [9], it is more challenging to optimize process parameters for the bottom-blowing lead oxidation smelting process. How to optimize process parameters is a crucial and challenging issue in enhancing the bottom-blowing lead smelting process.

These parameters are closely related to the thermodynamics of the bottom-blowing lead smelting process. Oxygen-enriched bottom-blowing smelting is a high-temperature, multi-phase, and multicomponent complex system. Conventional static experiments cannot be used to carry out systematic thermodynamic analysis [10]. Due to the vigorous agitation of oxygen-enriched air on the high-temperature molten pool, the mass and heat transfer processes in the reactor are intensified, which brings the reaction close to

thermodynamic equilibrium rapidly [8,11–14]. Therefore, using a computer to build thermodynamic models to study the fundamental theory of the lead smelting process has increasingly attracted the attention of researchers. Constructing thermodynamic models is mainly based on the minimum Gibbs free energy method [11] or the chemical equilibrium constant method [15,16]. Chen et al. [17] established thermodynamic models for the oxygen-enriched bottom-blowing lead oxidation smelting process with the minimum Gibbs free energy method. Tan et al. [18] and Zhang et al. [19] constructed thermodynamic models for the QSL process based on the chemical equilibrium constant method. However, the existing QSL thermodynamic models did not consider As, Sb, Bi and other impurity elements. They were unable to adapt to the complicated raw materials [9]. Therefore, we used the chemical equilibrium constant method to construct a thermodynamic model, taking into account the impurity elements such as As, Sb, Bi, Mg, and Al.

In the lead smelting research, there were many papers that simulated lead smelting by constructing thermodynamic models [18–20], but few of them further developed thermodynamic models into visual operation interfaces. The learning and usage of thermodynamic models became more challenging without visual operation interfaces. In copper smelting, Wang et al. [12] constructed a thermodynamic model for bottom-blown copper smelting and further developed the SKSSIM simulation software (SKSSIM v1.0) with C# program language. The software significantly dropped the difficulty of model usage and improved the efficiency of optimizing process parameters. However, with the increasing importance of the bottom-blowing lead smelting process in China, there is still no researcher who has constructed a thermodynamic model with a visual operating interface for the bottom-blowing lead smelting process. In this study, we adopted the MetCal v7.81 [21,22], which features a modular construction for thermodynamic models, to rapidly develop a thermodynamics simulation system with visual operation interfaces. This simulation system integrates the process flowchart and the calculation flowchart, providing an intuitive visualization of the bottom-blowing lead oxidation smelting process. It is expected to provide a useful tool for thermodynamic analysis.

In this study, we used the chemical equilibrium constant method and the MetCal v7.81 to develop a multi-phase equilibrium thermodynamic model and simulation system for the oxygen-enriched bottom-blowing lead oxidation smelting process. This process is based on the multi-phase equilibrium principle and the mechanism of the bottom-blowing lead oxidation smelting process. We simulated the equilibrium product composition and key technical indicators and compared them with industrial data in order to verify the accuracy of the model. It is expected to provide an effective tool for predicting the output of the bottom-blowing lead oxidation smelting process, revealing the impurity distribution behavior pattern, and optimizing the process parameters.

## 2. Modeling Principles

### 2.1. Lead Bottom-Blowing Oxidation Smelting Process

The lead smelting process has three stages: oxidation smelting, reduction smelting, and slag fuming. We studied the bottom-blowing lead oxidation smelting process. The oxygen-enriched bottom-blowing lead smelting process took place in a bottom-blowing furnace. The main structure is shown in Figure 1. After mixing and granulation, the carbide slag, lead glass, lead concentrate, lead mud, zinc leaching residue, return dust, and coal were added to the furnace from the air-sealed feeding port above the furnace at a certain ratio. A specific ratio of industrial oxygen was injected into the molten pool from the oxygen lance at the bottom of the furnace. The injected oxygen formed a large number of microbubbles, which entered the molten pool and dispersed throughout the melt. At the same time, the injected oxygen played a stirring role, forming good heat and mass transfer conditions. This enables the reaction to quickly approach an equilibrium state [13,14,17]. The granular material added from the feed opening fell onto the surface of the molten pool and was quickly swept into the molten pool. Under high oxygen potential, a part of lead oxide and lead sulfide interacted to form metal lead. Part of the lead oxide and silica reacted

to form slag. The sulfides of iron and zinc were oxidized, and then, the metal oxides reacted with silica and calcium oxide to form the slag. The melted lead and lead-rich slag formed a lead layer and a slag layer in the molten pool because of the different densities. Finally, we obtained crude lead containing less than 0.5% S, lead-rich slag containing about 40% Pb, and flue gas containing 8–12% SO<sub>2</sub>. Part of the melt was lifted up by a high-pressure jet stream, forming oxidized dust. The furnace was kept at a specific negative pressure so that the high-temperature flue gas could enter the waste heat boiler. The crude lead was discharged into the refining furnace through the crude lead port. The slag port released the lead-rich slag into the reduction furnace.

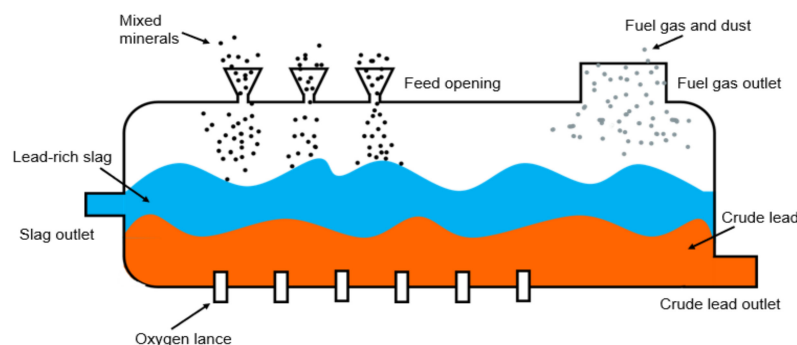


**Figure 1.** Schematic diagram of the structure of a bottom-blowing lead oxidation furnace.

## 2.2. Modeling Assumptions

According to the reaction mechanism of the bottom-blowing lead oxidation smelting process, the products of the lead concentrate oxidation smelting process consisted of primary crude lead, lead-rich slag, flue gas, and dust. In constructing a multi-phase equilibrium model for oxidation smelting, the equilibrium product consisted of only primary crude lead, lead-rich slag, and flue gas, while the dust consisted of mechanical dust and flue gas cooling dust. We assumed that the chemical composition of the product was at equilibrium, which is shown in Table 1.

**Table 1.** The chemical composition of the product.

Phases	Chemical Components
Primary crude lead (Ld)	Pb, PbS, Zn, ZnS, Cu, CuS <sub>0.5</sub> , Fe, FeS, As, Bi, Sb, Ag, Au, Cd, Others; PbO, PbS, PbSO <sub>4</sub> , PbSiO <sub>3</sub> , ZnO, Zn <sub>2</sub> SiO <sub>4</sub> , ZnFe <sub>2</sub> O <sub>4</sub> , CuO <sub>0.5</sub> , CuS <sub>0.5</sub> , CuFe <sub>2</sub> O <sub>4</sub> , FeO, FeO <sub>1.33</sub> , FeS, <sub>2</sub> FeO•SiO <sub>2</sub> , CaO, MgO, AlO <sub>1.5</sub> , SiO <sub>2</sub> , KO <sub>0.5</sub> , NaO <sub>0.5</sub> , BaSO <sub>4</sub> , AsO <sub>1.5</sub> , BiO <sub>1.5</sub> , SbO <sub>1.5</sub> , CdO, AgO <sub>0.5</sub> , Au, Others;
Lead-rich slag (Sl)	O <sub>2</sub> , Pb, PbO, PbS, Zn, ZnO, ZnS, CdO, CdS, SO <sub>2</sub> , S <sub>2</sub> , CO, CO <sub>2</sub> , N <sub>2</sub> , AsO <sub>1.5</sub> , AsS <sub>1.5</sub> , SbO <sub>1.5</sub> , SbS <sub>1.5</sub> , H <sub>2</sub> O; Ca(OH) <sub>2</sub> , CaCO <sub>3</sub> , CaSO <sub>4</sub> , SiO <sub>2</sub> , AlO <sub>1.5</sub> , FeO <sub>1.33</sub> , MgSiO <sub>3</sub> , K <sub>2</sub> SiO <sub>3</sub> , Na <sub>2</sub> SiO <sub>3</sub> , H <sub>2</sub> O, PbO•SiO <sub>2</sub> , CaSiO <sub>3</sub> , PbS, PbSO <sub>4</sub> , ZnS, CuS <sub>0.5</sub> , FeS <sub>2</sub> , FeO <sub>1.5</sub> , AsS <sub>1.5</sub> , SbS <sub>1.5</sub> , BiS <sub>1.5</sub> , CdS, AgO <sub>0.5</sub> , Au, PbO, BaSO <sub>4</sub> , ZnSO <sub>4</sub> , FeSO <sub>4</sub> , ZnO, CuO, FeO, CaO, Ag, AsO <sub>1.5</sub> , SbO <sub>1.5</sub> , BiO <sub>1.5</sub> , CdO, PbSiO <sub>3</sub> , Zn <sub>2</sub> SiO <sub>4</sub> , Ag <sub>2</sub> SO <sub>4</sub> , CuO <sub>0.5</sub> , Pb, Zn, Cu, Fe, FeS, As, Bi, Sb, Cd, ZnFe <sub>2</sub> O <sub>4</sub> , CuFe <sub>2</sub> O <sub>4</sub> , 2FeO•SiO <sub>2</sub> , MgO, KO <sub>0.5</sub> , NaO <sub>0.5</sub> , Others;
Flue gas (Gas)	
Dust (Dt)	

## 2.3. Model Construction

According to the chemical equilibrium constant method, also known as the K-value method, the system reaches equilibrium at constant temperature and pressure. We established a nonlinear system of equations based on the chemical equilibrium constant equation and the mass conservation equation for each element. Then, we solved the nonlinear system of equations algorithmically to obtain the amount of each component of each phase in the system.

From the model assumptions and the phase rule:

$$P + F = C + 2 \quad (1)$$

where  $P$  is the number of phases,  $F$  is the degree of freedom, and  $C$  is the number of components.

The bottom-blowing lead oxidation smelting system has 22 components and 60 chemical species. The system has a set of linearly independent molecular formula vectors, which are called independent species, and the remaining species are called dependent species. We selected the elements Pb, Zn, Cu, Fe, S, As, Sb, Bi, Ag, Au, Cd, Mg, Al, K, Na, Ba, O, C, H, and N and the oxides SiO<sub>2</sub> and CaO as the “components,” which formed the stoichiometry matrix for the 22 independent species shown in Table A1 of Appendix A and the stoichiometry matrix for the 38 dependent species shown in Table A2 of Appendix A. The stoichiometric coefficient matrix of the reactions could be obtained from the stoichiometry matrix of the independent species and dependent species. The chemical reactions consisting of a linearly independent set of row vectors in the stoichiometric coefficient matrix of reactions formed the independent reaction equations. Assuming that the number of elements contained in the reaction system was  $N_e$  and the number of compound species was  $N_c$ , the amount of each species within the system was determined by independent reaction equations, where the independent reaction number  $N_b$  is equal to  $N_c - N_e$  and the  $N_b$  independent reactions can be expressed as follows:

$$(V_{j,i})(A_{i,k}) = (B_{j,k}) \quad (2)$$

where  $V_{j,i}$  is the stoichiometric coefficient matrix of reactions,  $A_{i,k}$  and  $B_{j,k}$  are the matrices of the constituent components of the independent species and the dependent species, respectively; and  $i$ ,  $j$ , and  $k$  denote the independent species number, the dependent species number, and the species number, respectively.

According to the rules of matrix operations,  $V_{j,i}$  can be obtained as follows:

$$(V_{j,i}) = (B_{j,k})(U_{k,i}) \quad (3)$$

where  $(U_{k,i})$  denotes the inverted matrix of  $(A_{i,k})$  and must be calculable.  $i \in [1, 22]$ ,  $k \in [1, 22]$ , and  $j \in [1, 38]$ .

The chemical equilibrium constants  $K_j$  for the 38 independent reactions (Table 2) of the 38 dependent species produced from the 22 independent species are given by

$$K_j = \exp\left(-\frac{(\Delta G_{bj}^0 - \sum V_{ji}\Delta G_{ai}^0)}{RT}\right) \quad (4)$$

where  $R$  is the molar gas constant,  $T$  is the equilibrium temperature of the system,  $\Delta G_{ai}^0$  is the standard Gibbs free energy of formation of  $i$ th independent species, and  $\Delta G_{bj}^0$  is the standard Gibbs free energy of formation of the  $j$ th dependent species.

When the bottom-blowing lead oxidation smelting reaction system reaches equilibrium, the resulting relationship between the 22 independent species and the 38 dependent species can be expressed as follows:

$$Y_j = \left(\frac{Z_{m,j}}{\gamma_j}\right) (K_j) \prod_i \left(\frac{\gamma_i X_i}{Z_{m,i}}\right)^{V_{ji}} \quad (5)$$

where  $X_i$  is the mole number of the  $i$ th independent species;  $\gamma_i$  is the activity factor of the  $i$ th independent species;  $Z_{m,i}$  is the mole number of the phase to which the  $i$ th independent species belongs;  $Y_j$  is the mole number of the  $j$ th dependent species;  $\gamma_j$  is the activity factor of the  $j$ th dependent species; and  $Z_{m,j}$  is the mole number of the phase to which the  $j$ th dependent species belongs.

**Table 2.** Equilibrium reactions for the bottom-blowing lead oxidation smelting process.

Equilibrium Reaction	K <sub>j</sub>	Equilibrium Reaction	K <sub>j</sub>
$Pb_{(Ld)} + 0.5O_{2(gas)} = PbO_{(Sl)}$	K <sub>1</sub>	$Zn_{(gas)} + 0.5O_{2(gas)} = ZnO_{(gas)}$	K <sub>20</sub>
$PbS_{(Ld)} + O_{2(gas)} = Pb_{(Sl)} + SO_{2(gas)}$	K <sub>2</sub>	$ZnS_{(gas)} + 1.5O_{2(gas)} = ZnO_{(gas)} + SO_{2(gas)}$	K <sub>21</sub>
$Zn_{(Ld)} + 0.5O_{2(gas)} = ZnO_{(Sl)}$	K <sub>3</sub>	$S_{2(gas)} + 2O_{2(gas)} = 2SO_{2(gas)}$	K <sub>22</sub>
$CuS_{0.5(Sl)} + 1.5O_{2(gas)} = CuO_{0.5(Sl)} + 0.5SO_{2(gas)}$	K <sub>4</sub>	$CO_{(gas)} + 0.5O_{2(gas)} = CO_{2(gas)}$	K <sub>23</sub>
$FeS_{(Ld)} + 1.5O_{2(gas)} = FeO_{(Sl)} + SO_{2(gas)}$	K <sub>5</sub>	$FeO_{(Sl)} + 0.165O_{2(gas)} = FeO_{1.33(Sl)}$	K <sub>24</sub>
$Pb_{(Ld)} = Pb_{(gas)}$	K <sub>6</sub>	$FeS_{(Sl)} + 1.5O_{2(gas)} = FeO_{(Sl)} + SO_{2(gas)}$	K <sub>25</sub>
$Cd_{(Ld)} + 0.5O_{2(gas)} = CdO_{(Sl)}$	K <sub>7</sub>	$CuS_{0.5(Sl)} + 0.75O_{2(gas)} = CuO_{0.5(Sl)} + 0.5SO_{2(gas)}$	K <sub>26</sub>
$Pb_{(gas)} + 0.5O_{2(gas)} = PbO_{(gas)}$	K <sub>8</sub>	$PbS_{(Sl)} = PbS_{(gas)}$	K <sub>27</sub>
$PbS_{(Sl)} + 2PbO_{(Sl)} = 3Pb_{(Ld)} + SO_{2(gas)}$	K <sub>9</sub>	$CdO_{(Sl)} = CdO_{(gas)}$	K <sub>28</sub>
$AsO_{1.5(Sl)} = AsO_{1.5(gas)}$	K <sub>10</sub>	$FeO_{(Sl)} + CO_{(gas)} = Fe_{(Ld)} + CO_{2(gas)}$	K <sub>29</sub>
$AsS_{1.5(gas)} + 2.25O_{2(gas)} = AsO_{1.5(gas)} + 1.5SO_{2(gas)}$	K <sub>11</sub>	$ZnS_{(Ld)} + 1.5O_{2(gas)} = ZnO_{(Sl)} + SO_{2(gas)}$	K <sub>30</sub>
$As_{(Ld)} + 0.75O_{2(gas)} = AsO_{1.5(Sl)}$	K <sub>12</sub>	$ZnO_{(Sl)} + 0.5SiO_{2(Sl)} = 0.5Zn_2SiO_4(Sl)$	K <sub>31</sub>
$Bi_{(Ld)} + 0.75O_{2(gas)} = BiO_{1.5(Sl)}$	K <sub>13</sub>	$Zn_{(Ld)} = Zn_{(gas)}$	K <sub>32</sub>
$SbO_{1.5(Sl)} = SbO_{1.5(gas)}$	K <sub>14</sub>	$CuO_{0.5(Sl)} + 0.5CO_{(gas)} = Cu_{(Ld)} + 0.5CO_{2(gas)}$	K <sub>33</sub>
$SbS_{1.5(gas)} + 2.25O_{2(gas)} = SbO_{1.5(gas)} + 1.5SO_{2(gas)}$	K <sub>15</sub>	$Au_{(Ld)} = Au_{(Sl)}$	K <sub>34</sub>
$Sb_{(Ld)} + 0.75O_{2(gas)} = SbO_{1.5(Sl)}$	K <sub>16</sub>	$PbO_{(Sl)} + SiO_{2(Sl)} = PbSiO_3(Sl)$	K <sub>35</sub>
$AgO_{0.5(Ld)} + 0.5CO_{(gas)} = Ag_{(Ld)} + 0.5CO_{2(gas)}$	K <sub>17</sub>	$FeO_{(Sl)} + SiO_{2(Sl)} = FeO \cdot SiO_2(Sl)$	K <sub>36</sub>
$PbS_{(Sl)} + PbSO_4(Sl) = 2Pb_{(Ld)} + 2SO_{2(gas)}$	K <sub>18</sub>	$ZnO_{(Sl)} + 2FeO_{1.33(Sl)} + 0.167O_{2(gas)} = ZnFe_2O_4(Sl)$	K <sub>37</sub>
$CdS_{(gas)} + 1.5O_{2(gas)} = CdO_{(gas)} + SO_{2(gas)}$	K <sub>19</sub>	$CuO_{0.5(Sl)} + 2FeO_{(Sl)} + 0.75O_{2(gas)} = CuFe_2O_4(Sl)$	K <sub>38</sub>

The total mole number of the m product phase in Equation (5),  $Z_m$ , is given by

$$Z_m = \sum_{i(m)} X_i + \sum_{j(m)} Y_j \quad (6)$$

where  $i(m)$  means that only the independent species  $i$  that belongs to the product phase  $m$  is included in the summation; similarly,  $j(m)$  means that only the dependent species  $j$  that belongs to the product phase  $m$  is included in the summation.

According to the law of conservation of mass, the mole number of each element is calculated as follows:

$$Q_k = \sum_i A_{i,k} X_i + \sum_j B_{j,k} Y_j \quad (7)$$

where  $Q_k$  is the mole number of element  $k$ .

The amount of each species in each phase at the equilibrium of this system can be obtained by solving the system of nonlinear equations consisting of Equations (5)–(7) according to the Newton–Raphson algorithm.

### 3. Basic Data and Simulation System

#### 3.1. Raw Materials and Their Compositions

The main raw materials input included carbide slag, lead glass, lead concentrate, lead mud, zinc leaching slag, return dust, coal, air, and industrial oxygen (oxygen volume concentration of 95%). Based on the elements analysis data of raw material in the factory and the composition of common industrial raw materials [23–25], models for each raw material were constructed using the MetCal v7.81 to calculate their composition, as shown in Tables 3–9.

**Table 3.** Chemical composition of carbide slag (wt%).

Ca(OH) <sub>2</sub>	CaCO <sub>3</sub>	CaSO <sub>4</sub>	SiO <sub>2</sub>	Al <sub>2</sub> O <sub>3</sub>	Fe <sub>3</sub> O <sub>4</sub>
51.56	0.022	0.25	1.14	0.51	0.20
MgSiO <sub>3</sub>	K <sub>2</sub> SiO <sub>3</sub>	Na <sub>2</sub> SiO <sub>3</sub>	H <sub>2</sub> O	Other	
1.49	0.089	0.18	33	12.87	

**Table 4.** Chemical composition of lead concentrate (wt%).

PbS	PbSO <sub>4</sub>	ZnS	Cu <sub>2</sub> S	FeS <sub>2</sub>	Fe <sub>2</sub> O <sub>3</sub>	CaCO <sub>3</sub>	SiO <sub>2</sub>
51.16.	5.19	7.88	1.49	15.59	2.57	2.23	5.07
As <sub>2</sub> S <sub>3</sub>	Sb <sub>2</sub> S <sub>3</sub>	Bi <sub>2</sub> S <sub>3</sub>	CdS	Ag <sub>2</sub> O	Au	H <sub>2</sub> O	Other
0.73	0.40	0.25	0.03	0.15	0.0003	7.2	0.0597

**Table 5.** Chemical composition of zinc leaching slag (wt%).

PbS	PbSO <sub>4</sub>	PbSiO <sub>3</sub>	ZnSO <sub>4</sub>	Zn <sub>2</sub> SiO <sub>4</sub>	ZnO	ZnS	CdO
7.24	32.12	4.28	6.23	5.71	2.43	2.92	1.11
Fe <sub>3</sub> O <sub>4</sub>	CaSO <sub>4</sub>	SiO <sub>2</sub>	Al <sub>2</sub> O <sub>3</sub>	AgSO <sub>4</sub>	H <sub>2</sub> O	Other	
0.39	3.30	0.22	1.07	0.04	2	30.94	

**Table 6.** Chemical composition of return dust (wt%).

PbS	PbO	PbSO <sub>4</sub>	ZnSO <sub>4</sub>	ZnO	CuO	FeO
0.33	5.34	50.85	32.40	2.33	0.03	0.37
CaO	SiO <sub>2</sub>	Ag	Au	As <sub>2</sub> O <sub>3</sub>	As <sub>2</sub> S <sub>3</sub>	Sb <sub>2</sub> O <sub>3</sub>
0.3	0.1	0	0	0.09	0.55	0.31
Sb <sub>2</sub> S <sub>3</sub>	Bi <sub>2</sub> O <sub>3</sub>	Bi <sub>2</sub> S <sub>3</sub>	CdO	CdS	Other	
0.05	0.39	0.06	5.89	0.44	0.17	

**Table 7.** Chemical composition of lead mud (wt%).

PbO	PbSO <sub>4</sub>	BaSO <sub>4</sub>	CaSO <sub>4</sub>	ZnSO <sub>4</sub>	FeSO <sub>4</sub>	SiO <sub>2</sub>	H <sub>2</sub> O	Other
18.38	54.04	1.52	0.52	0.22	0.04	0.27	10	15.01

**Table 8.** Chemical composition of lead glass (wt%).

PbS·SiO <sub>2</sub>	SiO <sub>2</sub>	CaSiO <sub>3</sub>	K <sub>2</sub> SiO <sub>3</sub>	Na <sub>2</sub> SiO <sub>3</sub>	MgSiO <sub>3</sub>	H <sub>2</sub> O	Other
33.18	19.88	9.36	16.26	8.42	4.43	0	8.47

**Table 9.** Chemical composition of coal (wt%).

C	CH <sub>4</sub>	CO <sub>2</sub>	H <sub>2</sub>	N <sub>2</sub>	H <sub>2</sub> S	Fe <sub>2</sub> O <sub>3</sub>
80	5.05	1.88	0.98	1.15	0.53	1.00
CaO	MgO	Al <sub>2</sub> O <sub>3</sub>	H <sub>2</sub> O	Other	SiO <sub>2</sub>	
0.24	0.05	3.28	0.39	0.64	4.81	

### 3.2. Thermodynamic Basic Data

The Gibbs free energy of equilibrium product phase components in the bottom-blowing lead oxidation smelting process can be calculated by Equation (8), which is derived from Kirchhoff's formula and the relationship between standard molar reaction entropy and temperature in Appendix B. The standard Gibbs free energy and other relevant thermodynamic parameters for each product component were obtained through the MetCal v7.81, as shown in Table A3 of Appendix A. To eliminate the influence of reaction kinetics,

the product phase activity coefficient was corrected based on the literature [11,17–19,26], as shown in Table A4 of Appendix A. The activity factor of the components in flue gas was 1.

$$\Delta G_T^\theta = \Delta H_{298}^\theta - T \cdot \Delta S_{298}^\theta + \int_{298}^T c_p dT - T \int_{298}^T \frac{c_p}{T} dT \quad (8)$$

### 3.3. System Development

The model described in Section 2.3 was calculated according to the algorithm flowchart shown in Figure 2. Then, according to Equation (9), we considered the thermal equilibrium of this smelting process and applied the MetCal v7.81 to develop a thermodynamic simulation system for bottom-blowing lead oxidation smelting, as shown in Figure 3.

$$\sum_i^{n_A} \Delta H_{298, A_i} + \sum_i^{n_A} \int_{298}^{T_i} c_{p, A_i} dT = \sum_j^{n_B} \Delta H_{298, B_j} + \sum_j^{n_B} \int_{298}^{T_j} c_{p, B_j} dT + Q_{\text{Loss}} \quad (9)$$

where  $A_i$  is the  $i$ th reactant;  $n_A$  is the amount of reactant;  $T_i$  is the initial temperature of the reactant  $A_i$ ;  $B_j$  is the  $j$ th product;  $n_B$  is the amount of product;  $T_j$  is the temperature of product  $B_j$ ;  $\Delta H$  is the enthalpy;  $c_p$  is the specific heat at constant pressure; and  $Q_{\text{Loss}}$  is the heat loss.

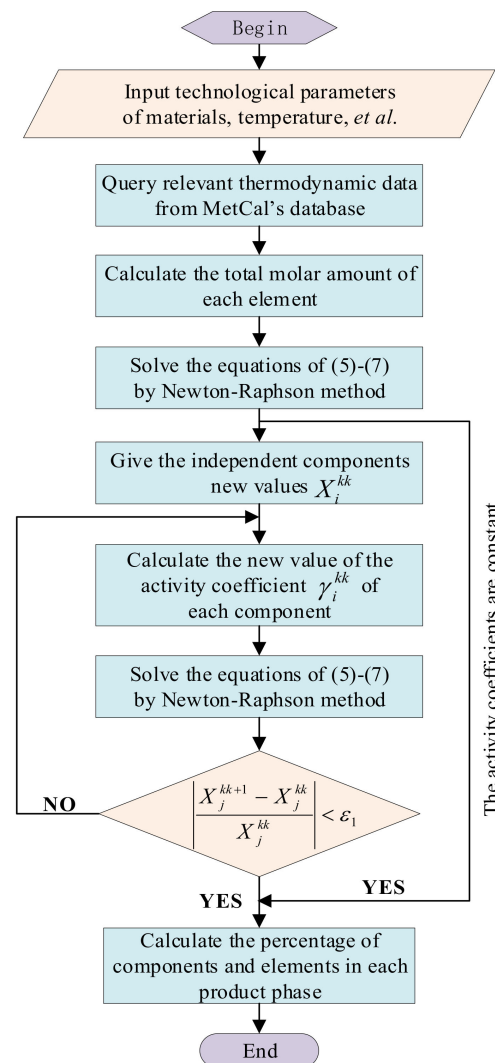


Figure 2. Calculation flowchart of thermodynamic model.

### Multiphase Equilibrium Simulation System for Lead Oxygen-Rich Bottom Blowing Oxidative Smelting

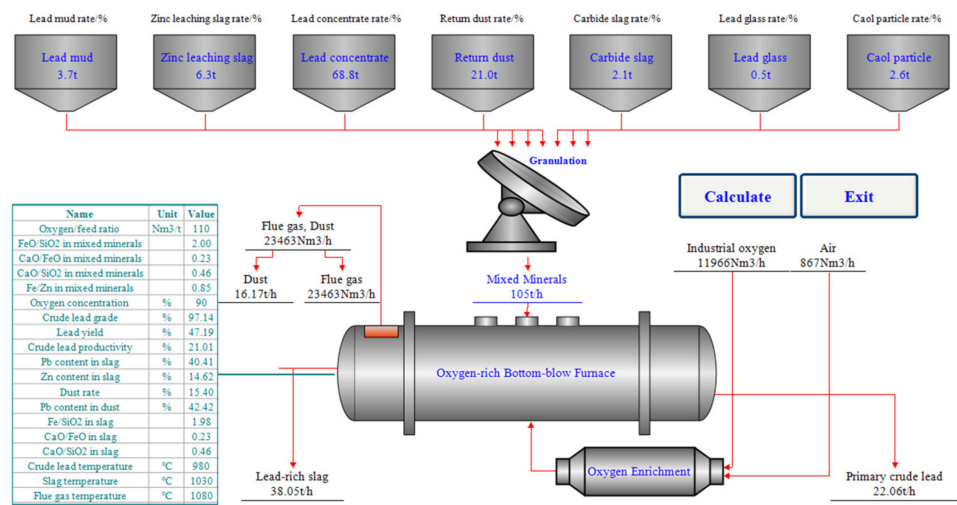


Figure 3. Thermodynamic simulation system for bottom-blowing lead oxidation smelting.

## 4. Model Validation

### 4.1. Calculation Conditions

We used the developed thermodynamic simulation system for bottom-blowing lead oxidation smelting to calculate the equilibrium product composition for a lead smelter in China. We used their average operating parameters from December 2021 to February 2022 as the calculating conditions. The total feedstock input was 105 t/h, which was granulated by 65.5% lead concentrate, 2% calcium carbide slag, 3.5% lead mud, 6% zinc leach slag, 20% return dust, 0.5% lead glass, and 2.5% coal. The oxygen-enriched concentration was 90%. The oxygen/feed ratio was 110 Nm<sup>3</sup>/t, and the melting temperature was obtained from heat balance calculations. We assumed that the primary crude lead temperature was 50 °C lower than the lead-rich slag temperature and the flue gas and dust temperature was 50 °C higher than the lead-rich slag temperature.

### 4.2. Calculation Result Verification

Based on the industrial data of a Chinese lead smelter from December 2021 to February 2022, the industrial elements analysis data of primary crude lead, lead-rich slag, and dust were averaged and compared with the model calculated data. The results are shown in Figure 4.

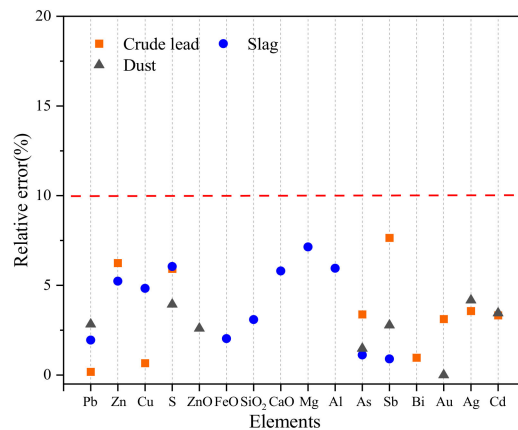


Figure 4. Relative error of product element composition between calculated values and industrial data.

The calculated values of the elements in the product, excluding some elements that were not detected in production, closely matched the industrial data. The relative errors of the elemental compositions of Pb, Zn, Cu, S, As, Sb, Bi, and Cd in the primary crude lead were 0.18%, 6.25%, 0.66%, 5.92%, 3.38%, 7.65%, 0.97%, and 3.33%, respectively. The relative errors of the elemental compositions of Pb, Zn, Cu, S, FeO, SiO<sub>2</sub>, CaO, Mg, Al, As, and Sb in the lead-rich slag were 1.95%, 5.23%, 4.83%, 6.05%, 2.03%, 3.09%, 5.80%, 7.14%, 5.95%, 1.12%, and 0.90%, respectively. The relative errors of the compositions of Pb, S, ZnO, As, Sb, Ag and Cd in dust were 2.83%, 3.94%, 2.60%, 1.48%, 2.78%, 4.17% and 3.45%, respectively.

According to the results of the data presented in Figure 4, the relative error of element Sb in primary crude lead was the largest, 7.65%. In lead-rich slag, the relative error of Mg was the largest, 7.14%, and the relative error of Ag in dust was the largest, 4.17%. The relative errors of some elements are relatively large, which may be caused by three factors. Firstly, there is a lack of thermodynamic parameters for some elements in the high-temperature smelting system of lead, and the deviation of activity coefficients affects the accuracy of the calculated results. Secondly, the model assumed that the oxidation smelting process is at a constant temperature, but in reality, the temperature of the oxidation smelting process is in a dynamic state of change. Finally, during the iterative calculation of the model, errors will gradually accumulate, and these errors will gradually accumulate as iterations increase. The average relative error of all elements was 3.76%. The error range of these results was small, and the results showed that the model reflected the smelting characteristics of bottom-blowing lead oxidation and provided a useful tool for subsequent thermodynamic analysis of the system.

The calculated values of key technical indicators, such as the iron–silica ratio and the calcium–silica ratio in slag, soot rate, primary crude lead productivity, and lead-rich slag temperature, were 1.98, 0.46, 15.4%, 21.01%, and 1030 °C, respectively, and the corresponding production averages were 1.90, 0.45, 15%, 24%, and 1150 °C, with relative errors of 4.21%, 2.22%, 2.66%, 12.45%, and 10.43%, respectively. The main reasons for the deviations in the primary crude lead productivity and the temperature of the lead-rich slag are as follows: the heat transfer behavior during the lead oxidation smelting process is very complex, including convection, diffusion, radiation, and other heat transfer modes between the furnace shell and furnace lining, as well as between the outer wall of the furnace shell and the outer environment. Therefore, there were errors in the calculation of thermal equilibrium, which in turn led to errors in the primary crude lead productivity. The results obtained by the constructed thermodynamic simulation system for the bottom-blowing lead oxidation smelting process closely reflected the actual production situation and reflected the bottom-blowing lead oxidation smelting production process, which can be used as an effective tool for subsequent industrial production parameter optimization.

## 5. Conclusions

- (1) Based on the mechanism of the bottom-blowing lead oxidation smelting process, we constructed a multi-phase equilibrium mathematical model of the bottom-blowing lead oxidation smelting process using the chemical equilibrium constant method. We developed a bottom-blowing lead oxidation smelting thermodynamic simulation system based on the MetCal v7.81 and provided an effective tool for the thermodynamic calculation of the process.
- (2) We validated the model using the average operating parameters of the bottom-blowing lead oxidation smelting of a Chinese lead smelter as the calculation conditions. The average relative error of the calculation value of the mass fraction in the crude lead, lead-rich slag, and dust was 3.76%. The results closely matched the production values, indicating that the model could reflect the multi-phase reaction characteristics of the bottom-blowing lead oxidation smelting process. Therefore, it is a useful tool for the subsequent thermodynamic analysis of the system.
- (3) The calculated values of the key technical indicators of the lead bottom-blowing smelting process had small errors with the average measured values of industrial

production. The average relative error of important technical indicators, including dust rate, crude lead productivity, lead-rich slag temperature, slag iron–silica ratio ( $R_{Fe/SiO_2}$ ), and slag calcium–silica ratio ( $R_{CaO/SiO_2}$ ), was 6.39%, which indicated that the constructed model closely reflected the actual lead bottom-blowing smelting process and had the potential to improve the production process and optimize the process parameters.

**Author Contributions:** Conceived and designed the experiments, M.L. and M.Y.; performed the experiments, M.Y. and X.C.; analyzed the data, M.Y. and X.C.; searched the relevant literature and data, M.Y., X.C. and M.L.; wrote the paper, X.C.; reviewed and contributed to the final manuscript, F.L., J.H., M.L. and X.C. All authors have read and agreed to the published version of the manuscript.

**Funding:** This research was funded by the National Key Research and Development Program (No. 2022YFC2904201), the Natural Science Foundation of Jiangxi Province of China (No. 20212BAB204026), the China Baowu Low Carbon Metallurgy Innovation Foundation (No. BWLCF202121), the China Postdoctoral Science Foundation (No. 2019M662268), National Nature Science Foundation of China (No. 52264047), Training Plan for Academic and Technical Leaders of Major Disciplines in Jiangxi Province (20225BCJ23009), Natural Science Foundation for Distinguished Young Scholars of Jiangxi Province (No.20232ACB214006), the Postdoctoral program of Jiangxi Province (No. 2018KY15), the Jiangxi Province Postdoctoral Daily Funding Project (No. 2019RC28).

**Data Availability Statement:** Data available on request from the authors.

**Acknowledgments:** The author is grateful to Qing Shu and Yanxin Wu for their advice on this paper. Special thanks to Henan Yuguang Gold Lead Co., Ltd. for providing the production data for this research.

**Conflicts of Interest:** The authors declare no conflict of interest.

## Appendix A

**Table A1.** Stoichiometry matrix for 22 independent species.

Com.	Phase	Pb	Zn	Cu	Fe	S	As	Sb	Bi	Ag	Au	Cd	Mg	Al	K	Na	Ba	SiO <sub>2</sub>	CaO	O	C	H	N
Pb	Ld	1	0	0	0	0	0	0	0	0	0	0	0	0	0	0	0	0	0	0	0	0	0
PbS	Ld	1	0	0	0	1	0	0	0	0	0	0	0	0	0	0	0	0	0	0	0	0	0
Zn	Ld	0	1	0	0	0	0	0	0	0	0	0	0	0	0	0	0	0	0	0	0	0	0
Cu	Ld	0	0	1	0	0	0	0	0	0	0	0	0	0	0	0	0	0	0	0	0	0	0
Fe	Ld	0	0	0	1	0	0	0	0	0	0	0	0	0	0	0	0	0	0	0	0	0	0
As	Ld	0	0	0	0	0	1	0	0	0	0	0	0	0	0	0	0	0	0	0	0	0	0
Sb	Ld	0	0	0	0	0	0	1	0	0	0	0	0	0	0	0	0	0	0	0	0	0	0
Bi	Ld	0	0	0	0	0	0	0	1	0	0	0	0	0	0	0	0	0	0	0	0	0	0
Ag	Ld	0	0	0	0	0	0	0	0	1	0	0	0	0	0	0	0	0	0	0	0	0	0
Au	Ld	0	0	0	0	0	0	0	0	0	1	0	0	0	0	0	0	0	0	0	0	0	0
Cd	Ld	0	0	0	0	0	0	0	0	0	0	1	0	0	0	0	0	0	0	0	0	0	0
PbO	Sl	1	0	0	0	0	0	0	0	0	0	0	0	0	0	0	0	0	0	1	0	0	0
PbSiO <sub>3</sub>	Sl	1	0	0	0	0	0	0	0	0	0	0	0	0	0	0	0	1	0	1	0	0	0
CaO	Sl	0	0	0	0	0	0	0	0	0	0	0	0	0	0	0	0	0	1	0	0	0	0
MgO	Sl	0	0	0	0	0	0	0	0	0	0	0	1	0	0	0	0	0	0	1	0	0	0
AlO <sub>1.5</sub>	Sl	0	0	0	0	0	0	0	0	0	0	0	0	1	0	0	0	0	0	1.5	0	0	0
KO <sub>0.5</sub>	Sl	0	0	0	0	0	0	0	0	0	0	0	0	0	1	0	0	0	0	0.5	0	0	0
NaO <sub>0.5</sub>	Sl	0	0	0	0	0	0	0	0	0	0	0	0	0	0	1	0	0	0	0.5	0	0	0
BaSO <sub>4</sub>	Sl	0	0	0	0	1	0	0	0	0	0	0	0	0	0	0	1	0	0	4	0	0	0
CO	Gas	0	0	0	0	0	0	0	0	0	0	0	0	0	0	0	0	0	0	1	1	0	0
N <sub>2</sub>	Gas	0	0	0	0	0	0	0	0	0	0	0	0	0	0	0	0	0	0	0	0	0	2
H <sub>2</sub> O	Gas	0	0	0	0	0	0	0	0	0	0	0	0	0	0	0	0	0	0	1	0	2	0

Table A2. Stoichiometry matrix for 38 dependent species.

Com.	Phase	Pb	Zn	Cu	Fe	S	As	Sb	Bi	Ag	Au	Cd	Mg	Al	K	Na	Ba	SiO <sub>2</sub>	CaO	O	C	H	N
ZnS	Ld	0	1	0	0	1	0	0	0	0	0	0	0	0	0	0	0	0	0	0	0	0	0
CuS <sub>0.5</sub>	Ld	0	1	0	0	0.5	0	0	0	0	0	0	0	0	0	0	0	0	0	0	0	0	0
FeS	Ld	0	0	0	1	1	0	0	0	0	0	0	0	0	0	0	0	0	0	0	0	0	0
PbS	Sl	1	0	0	0	1	0	0	0	0	0	0	0	0	0	0	0	0	0	0	0	0	0
PbSO <sub>4</sub>	Sl	1	0	0	0	1	0	0	0	0	0	0	0	0	0	0	0	0	0	4	0	0	0
ZnO	Sl	0	1	0	0	0	0	0	0	0	0	0	0	0	0	0	0	0	0	1	0	0	0
Zn <sub>2</sub> SiO <sub>4</sub>	Sl	0	2	0	0	0	0	0	0	0	0	0	0	0	0	0	0	1	0	2	0	0	0
ZnFe <sub>2</sub> O <sub>4</sub>	Sl	0	1	0	2	0	0	0	0	0	0	0	0	0	0	0	0	0	0	4	0	0	0
CuO <sub>0.5</sub>	Sl	0	0	1	0	0	0	0	0	0	0	0	0	0	0	0	0	0	0	0.5	0	0	0
CuS <sub>0.5</sub>	Sl	0	0	1	0	0.5	0	0	0	0	0	0	0	0	0	0	0	0	0	0	0	0	0
CuFe <sub>2</sub> O <sub>4</sub>	Sl	0	0	1	2	0	0	0	0	0	0	0	0	0	0	0	0	0	0	4	0	0	0
FeO	Sl	0	0	0	1	0	0	0	0	0	0	0	0	0	0	0	0	0	0	1	0	0	0
FeO <sub>1.33</sub>	Sl	0	0	0	1	0	0	0	0	0	0	0	0	0	0	0	0	0	0	1.33	0	0	0
FeS	Sl	0	0	0	1	1	0	0	0	0	0	0	0	0	0	0	0	0	0	0	0	0	0
2FeO·SiO <sub>2</sub>	Sl	0	0	0	2	0	0	0	0	0	0	0	0	0	0	0	0	1	0	2	0	0	0
SiO <sub>2</sub>	Sl	0	0	0	0	0	0	0	0	0	0	0	0	0	0	0	0	1	0	0	0	0	0
AsO <sub>1.5</sub>	Sl	0	0	0	0	0	1	0	0	0	0	0	0	0	0	0	0	0	0	1.5	0	0	0
SbO <sub>1.5</sub>	Sl	0	0	0	0	0	0	1	0	0	0	0	0	0	0	0	0	0	0	1.5	0	0	0
BiO <sub>1.5</sub>	Sl	0	0	0	0	0	0	0	1	0	0	0	0	0	0	0	0	0	0	1.5	0	0	0
CdO	Sl	0	0	0	0	0	0	0	0	0	1	0	0	0	0	0	0	0	0	1	0	0	0
AgO <sub>0.5</sub>	Sl	0	0	0	0	0	0	0	0	1	0	0	0	0	0	0	0	0	0	0.5	0	0	0
Au	Sl	0	0	0	0	0	0	0	0	0	1	0	0	0	0	0	0	0	0	0	0	0	0
O <sub>2</sub>	Gas	0	0	0	0	0	0	0	0	0	0	0	0	0	0	0	0	0	0	2	0	0	0
Pb	Gas	1	0	0	0	0	0	0	0	0	0	0	0	0	0	0	0	0	0	0	0	0	0
PbO	Gas	1	0	0	0	0	0	0	0	0	0	0	0	0	0	0	0	0	0	1	0	0	0
PbS	Gas	1	0	0	0	1	0	0	0	0	0	0	0	0	0	0	0	0	0	0	0	0	0
Zn	Gas	0	1	0	0	0	0	0	0	0	0	0	0	0	0	0	0	0	0	0	0	0	0
ZnO	Gas	0	1	0	0	0	0	0	0	0	0	0	0	0	0	0	0	0	0	1	0	0	0
ZnS	Gas	0	1	0	0	1	0	0	0	0	0	0	0	0	0	0	0	0	0	0	0	0	0
CdO	Gas	0	0	0	0	0	0	0	0	0	1	0	0	0	0	0	0	0	0	1	0	0	0
CdS	Gas	0	0	0	0	1	0	0	0	0	1	0	0	0	0	0	0	0	0	0	0	0	0
SO <sub>2</sub>	Gas	0	0	0	0	1	0	0	0	0	0	0	0	0	0	0	0	0	0	2	0	0	0
S <sub>2</sub>	Gas	0	0	0	0	2	0	0	0	0	0	0	0	0	0	0	0	0	0	0	0	0	0
CO <sub>2</sub>	Gas	0	0	0	0	0	0	0	0	0	0	0	0	0	0	0	0	0	0	2	1	0	0
AsO <sub>1.5</sub>	Gas	0	0	0	0	0	1	0	0	0	0	0	0	0	0	0	0	0	0	1.5	0	0	0
AsS <sub>1.5</sub>	Gas	0	0	0	0	1.5	1	0	0	0	0	0	0	0	0	0	0	0	0	0	0	0	0
SbO <sub>1.5</sub>	Gas	0	0	0	0	0	0	1	0	0	0	0	0	0	0	0	0	0	0	1.5	0	0	0
SbS <sub>1.5</sub>	Gas	0	0	0	0	1.5	0	1	0	0	0	0	0	0	0	0	0	0	0	0	0	0	0

Table A3. Thermodynamic parameters of species.

Component	State	$\Delta H_{298}^{\theta}/$ (kJ·mol <sup>-1</sup> )	$\Delta S_{298}^{\theta}/$ (J·K <sup>-1</sup> ·mol <sup>-1</sup> )	$c_p = a + b \times 10^{-3}T + c \times 10^5T^{-2} + d \times 10^{-6}T^2$			
				<i>a</i>	<i>b</i>	<i>c</i>	<i>d</i>
Pb	Liquid	3.873	70.506	27.159	1.029	0	0
Zn	Liquid	5.727	48.549	31.381	0	0	0
Cu	Liquid	8.028	34.236	32.845	0	0	0
Fe	Liquid	8.006	23.521	40.879	1.674	0	0
S	Liquid	0	32.071	32.005	-0.002	-0.038	0
As	Liquid	21.568	53.284	28.833	0	0	0
Sb	Liquid	17.531	62.712	31.381	0	0	0
Bi	Liquid	9.271	71.980	27.197	0	0	0
Cd	Liquid	5.607	60.717	29.707	0	0	0
Au	Liquid	0	47.489	-268.634	237.139	1418.47	-52.813
Ag	Liquid	6.393	43.220	33.473	0	0	0
PbO	Liquid	-202.249	73.379	65.000	0	0	0
PbS	Liquid	-93.143	84.129	66.946	0	0	0
ZnO	Liquid	-309.542	47.920	60.669	0	0	0
ZnS	Liquid	-203.005	58.661	49.753	4.448	-4.551	-0.005
AsO <sub>1.5</sub>	Liquid	-643.439	128.125	152.720	0	0	0
SbO <sub>1.5</sub>	Liquid	-675.490	143.628	156.904	0	0	0

Table A3. Cont.

Component	State	$\Delta H_{298}^{\theta}/$ (kJ·mol <sup>-1</sup> )	$\Delta S_{298}^{\theta}/$ (J·K <sup>-1</sup> ·mol <sup>-1</sup> )	$c_p = a + b \times 10^{-3}T + c \times 10^5T^{-2} + d \times 10^{-6}T^2$			
				<i>a</i>	<i>b</i>	<i>c</i>	<i>d</i>
BiO <sub>1.5</sub>	Liquid	-578.024	149.814	202.005	0	0	0
CdO	Liquid	-258.996	54.812	47.264	6.364	-4.908	0
Pb	Gas	195.205	175.377	28.063	-11.029	-9.310	4.728
PbO	Gas	68.139	240.048	41.612	-3.526	-20.136	1.014
PbS	Gas	127.959	251.416	37.350	0.194	-2.096	0.140
Zn	Gas	130.403	16.992	20.898	-0.133	-0.067	0.034
ZnO	Gas	136.518	242.811	37.671	-0.286	-1.985	0.735
ZnS	Gas	204.322	236.404	166.350	-85.742	-166.125	21.952
AsO <sub>1.5</sub>	Gas	-322.845	371.925	82.134	6.444	-5.356	0
AsS <sub>1.5</sub>	Gas	27.042	314.289	96.201	1.071	-8.213	0
SbO <sub>1.5</sub>	Gas	-708.564	129.903	180.004	0	0	0
SbS <sub>1.5</sub>	Gas	119.661	409.820	107.636	0.209	-7.255	0
CdO	Gas	127.003	231.570	43.560	-10.649	-11.819	5.291
CdS	Gas	175.662	244.987	36.257	-3.867	18.611	3.678
O <sub>2</sub>	Gas	0	205.154	34.860	1.312	-14.141	0.163
SO <sub>2</sub>	Gas	-296.820	248.226	54.781	3.350	-24.745	-0.241
S <sub>2</sub>	Gas	128.603	228.169	34.672	3.286	-2.816	-0.312
CO	Gas	-110.544	197.665	29.932	5.415	-10.814	-1.054
CO <sub>2</sub>	Gas	-393.515	213.774	54.437	5.116	-43.579	-0.806
N <sub>2</sub>	Gas	0	191.615	23.529	12.117	1.210	-3.076
H <sub>2</sub> O	Gas	-241.832	188.837	31.438	14.106	-24.952	-1.832

Table A4. Activity factor of species.

Com.	Phase	Activity Factor	Com.	Phase	Activity Factor	Com.	Phase	Activity Factor
Pb	Ld	0.0196	PbO	Sl	0.0036	PbO	Sl	0.0036
PbS	Ld	80	PbS	Sl	50	PbS	Sl	50
Zn	Ld	150	PbSO <sub>4</sub>	Sl	0.01	PbSO <sub>4</sub>	Sl	0.01
ZnS	Ld	1450	PbSiO <sub>3</sub>	Sl	0.01	PbSiO <sub>3</sub>	Sl	0.01
Cu	Ld	0.3	ZnO	Sl	1	ZnO	Sl	1
CuS <sub>0.5</sub>	Ld	40	Zn <sub>2</sub> SiO <sub>4</sub>	Sl	1	Zn <sub>2</sub> SiO <sub>4</sub>	Sl	1
Fe	Ld	10	ZnFe <sub>2</sub> O <sub>4</sub>	Sl	1	ZnFe <sub>2</sub> O <sub>4</sub>	Sl	1
FeS	Ld	10	CuO <sub>0.5</sub>	Sl	1	CuO <sub>0.5</sub>	Sl	1
As	Ld	50	CuS <sub>0.5</sub>	Sl	1	AsO <sub>1.5</sub>	Sl	1
Bi	Ld	4	CuFe <sub>2</sub> O <sub>4</sub>	Sl	1	BiO <sub>1.5</sub>	Sl	1
Sb	Ld	7	FeO	Sl	1	SbO <sub>1.5</sub>	Sl	1
Ag	Ld	1	FeO <sub>1.33</sub>	Sl	0.1	NaO <sub>0.5</sub>	Sl	1
Au	Ld	1	FeS	Sl	1	AgO <sub>0.5</sub>	Sl	1
Cd	Ld	8	2FeO·SiO <sub>2</sub>	Sl	1	Au	Sl	1
MgO	Sl	1	CaO	Sl	1	CdO	Sl	1
AlO <sub>1.5</sub>	Sl	1	BaSO <sub>4</sub>	Sl	1	Other	Sl	1
SiO <sub>2</sub>	Sl	1	KO <sub>0.5</sub>	Sl	1			

## Appendix B

The derivation of Equation (8) is as follows:

$$\Delta H_T^{\theta} = \Delta H_{298}^{\theta} + \int_{298}^T c_p \int dT$$

$$\Delta S_T^{\theta} = \Delta S_{298}^{\theta} + \int_{298}^T \frac{c_p}{T} dT$$

$$\Delta G_T^\theta = \Delta H_T^\theta - T \cdot \Delta S_T^\theta = \Delta H_{298}^\theta - T \cdot \Delta S_{298}^\theta + \int_{298}^T c_p dT - T \int_{298}^T \frac{c_p}{T} dT$$

## References

- Jiang, J.M. Situation and Development Trend of Lead Smelting Technology at Home and Abroad. *Energy Sav. Nonferrous Met.* **2013**, *29*, 4–8. (In Chinese)
- Chen, L.; Hao, Z.D.; Yang, T.Z.; Liu, W.F.; Zhang, D.C.; Zhang, L.; Bin, S.; Bin, W.D. A Comparison Study of the Oxygen-Rich Side Blow Furnace and the Oxygen-Rich Bottom Blow Furnace for Liquid High Lead Slag Reduction. *JOM* **2015**, *67*, 1123–1129. [[CrossRef](#)]
- Queneau, P.E. The QSL reactor for lead and its prospects for Ni, Cu and Fe. *JOM* **1989**, *41*, 30–35. [[CrossRef](#)]
- Chen, L.; Yang, T.Z.; Bin, S.; Liu, W.F.; Zhang, D.C.; Bin, W.D.; Zhang, L. An Efficient Reactor for High-Lead Slag Reduction Process: Oxygen-Rich Side Blow Furnace. *JOM* **2014**, *66*, 1664–1669. [[CrossRef](#)]
- Zhukov, V.P.; Kolmachikhin, B.V.; Kolmachikhina, É.B. Hydrogasdynamic Regularities of Melt Blowing in “Ausmelt” Furnace by Cold Modeling Methods. *Metallurgist* **2020**, *63*, 1220–1226. [[CrossRef](#)]
- Ramus, K.; Hawkins, P. Lead/acid battery recycling and the new Isasmelt process. *J. Power Sources* **1993**, *42*, 299–313. [[CrossRef](#)]
- Errington, W.J.; Edwards, J.S.; Hawkins, P. Isasmelt technology-current and future development. *J. South Afr. Inst. Min. Met.* **1997**, *97*, 161–167.
- Li, J.D.; Song, Y.P.; Zhou, P.; Ma, J.; Chen, Z.; Chai, L.Y. A RQPSO Algorithm for Multiphase Equilibrium Calculation in the KIVCET Process. *JOM* **2018**, *70*, 2893–2899. [[CrossRef](#)]
- Gu, Y.; Wang, J.P.; Wang, X.; Che, D.; Wu, Q.X. Situation and sustainable development proposals for lead resource development in China. *Resour. Ind.* **2018**, *20*, 39–46. (In Chinese) [[CrossRef](#)]
- Wang, Q.M.; Huang, M.X.; Wang, S.S.; Li, D.; Tian, Q.H.; Guo, X.Y. Research Progress on Thermodynamic Model of Typical Nonferrous Metal Smelting Process. *Nonferrous Met.* **2021**, *10*, 1–12. (In Chinese)
- Nagamori, M.; Chaubal, P.C. Thermodynamics of copper matte converting: Part III. Steady-state volatilization of Au, Ag, Pb, Zn, Ni, Se, Te, Bi, Sb, and As from slag, matte, and metallic copper. *Met. Trans. B* **1982**, *13*, 319–329. [[CrossRef](#)]
- Wang, Q.M.; Guo, X.Y.; Tian, Q.H.; Jiang, T.; Chen, M.; Zhao, B.J. Development and Application of SKSSIM Simulation Software for the Oxygen Bottom Blown Copper Smelting Process. *Metals* **2017**, *7*, 431. [[CrossRef](#)]
- Liu, F.K. Numerical Simulation and Optimization of Multiphase Flow in Bottom Blowing Lead Smelting Furnace. Master’s Thesis, Central South University, Changsha, China, 2013.
- Song, K.Z.; Jokilaakso, A. CFD Modeling of Multiphase Flow in an SKS Furnace with New Tuyere Arrangements. *Met. Mater. Trans. B Proc. Met. Mater. Proc. Sci.* **2022**, *53*, 253–272. [[CrossRef](#)]
- Shimpo, R.; Goto, S.; Ogawa, O.; Asakura, I. A Study on the Equilibrium between Copper Matte and Slag. *Can. Met. Q.* **1986**, *25*, 113–121. [[CrossRef](#)]
- Li, M.Z.; Zhou, J.M.; Tong, C.R.; Zhang, W.H.; Chen, Z.; Wang, J.L. Thermodynamic Modeling and Optimization of the Copper Flash Converting Process Using the Equilibrium Constant Method. *Met. Mater. Trans.* **2018**, *49*, 1794–1807. [[CrossRef](#)]
- Chen, L.; Wang, Z.H.; Chen, W.; Xiao, H.; Liu, W.F.; Zhang, D.C.; Yang, T.Z. Thermodynamic Simulation on Elements Distribution of Lead Concentrate Oxidative Smelting in Oxygen-Rich Bottom-Blow Smelting Process. *Nonferrous Met. Extr. Met.* **2018**, *9*, 1–6. (In Chinese) [[CrossRef](#)]
- Tan, P.F.; Zhang, C.F.; Zhang, R.Y. A Computer Model of QSL Lead Smelting Process. *J. Cent. South Univ. Sci. Technol.* **1996**, *5*, 40–43. (In Chinese)
- Zhang, C.F.; Tan, P.F.; Zeng, D.W.; Zhao, T.L. Computer simulation and theoretical analysis of QSL lead smelting process. *Nonferrous Met. Extr. Met.* **1997**, *1*, 13–16. (In Chinese)
- Shishin, D.; Hidayat, T.; Sultana, U.; Shevchenko, M.; Jak, E. Experimental measurement and thermodynamic model predictions of the distributions of Cu, As, Sb and Sn between liquid lead and PbO–FeO–Fe<sub>2</sub>O<sub>3</sub>–SiO<sub>2</sub> slag. *Int. J. Mater. Res.* **2020**, *111*, 733–743. [[CrossRef](#)]
- Chun, W.X.; Liang, W.J.; Qing, W.H. Research on the Mathematical Model of Local Equilibrium in the Top-Blown Smelting Process of Electronic Waste. *Metals* **2021**, *11*, 1500. [[CrossRef](#)]
- Li, M.Z.; Zhou, J.M.; Tong, C.R.; Zhang, W.H.; Li, H.S. Mathematical model of whole-process calculation for bottom-blowing copper smelting. *Met. Res. Technol.* **2018**, *115*, 107. [[CrossRef](#)]
- Song, J.B.; Xi, W.L.; Zhu, L.P.; Liu, S.H. Experimental study on oxygen-blowing co-smelting and desulfurization of lead concentrate with lead paste and lead glass. *China Nonferrous Met.* **2022**, *51*, 110–117. (In Chinese) [[CrossRef](#)]
- Li, D.B. *Morder Oxygen Bottom Blowing Lead Smelting Technology*; Metallurgical Industry Press: Beijing, China, 2020; pp. 71–76. (In Chinese)

25. Yao, G.; Guo, Q.; Li, Y.; Xu, Z.; Han, Z.; He, M.; Qi, T. An innovation technology for recovering silver and valuable metals from hazardous zinc leaching residue through direct reduction. *Miner. Eng.* **2022**, *188*, 107857. [[CrossRef](#)]
26. Wang, J.L.; Zhang, C.F.; Zhang, W.H. Multi-phase equilibrium model of lead flash smelting process. *J. Cent. South Univ. Sci. Technol.* **2012**, *43*, 429–434. (In Chinese)

**Disclaimer/Publisher’s Note:** The statements, opinions and data contained in all publications are solely those of the individual author(s) and contributor(s) and not of MDPI and/or the editor(s). MDPI and/or the editor(s) disclaim responsibility for any injury to people or property resulting from any ideas, methods, instructions or products referred to in the content.